Two types of scapolite in Evate carbonatite deposit (Mozambique): implications for magmatic versus metamorphic origins

Michaela Gajdošová[1], Monika Huraiová[1], Vratislav Hurai[2], Marek Slobodník[3] & Pete R. Siegfried[4]

[1]Department of Mineralogy and Petrology, Faculty of Natural Sciences, Comenius University in Bratislava, Ilkovičova 6, 842 15 Bratislava, Slovakia; michaela.gajdosova@uniba.sk
[2]Earth Science Institute, Slovak Academy of Sciences, Dúbravská cesta 9, 840 05 Bratislava, Slovakia
[3]Institute of Geological Sciences, Masaryk University, Kotlářská 267/2, 611 37 Brno, Czech Republic
[4]Geoafrica Prospecting Services cc, PO Box 24218, Windhoek, Namibia

AGEOS

Abstract: Two types of scapolite occur in the Evate carbonatite deposit – the largest resource of apatite in south-east Africa. Calc-silicate rocks composed of amphiboles (hastingsite, hornblende, actinolite, and pargasite), diopside, Ba-rich phlogopite, allanite, epidote, apatite, K-feldspar, titanite, and minor calcite, also contain scapolite with 62–74 mol. % of meionite – (*Me*) end-member, X_{Cl} = 0.06–0.17 and the crystallochemical formula corresponding to $(Ca_{2.46-2.99}Na_{1.00-1.47})_{\Sigma 4.00-4.20}Al_{4.62-5.04}Si_{6.95-7.37}O_{24}(Cl_{0.06-0.17}S_{0.18-0.26}C_{0.64-0.70})_{\Sigma 1.00}$. In contrast, carbonatite contains scapolite ranging from Na meionite to Ca marialite with 46–63 mol. % *Me*, X_{Cl} = 0.19–0.47 and the crystallochemical formula $(Na_{1.43-2.07}Ca_{1.82-2.50})_{\Sigma 3.97-4.11}Al_{4.29-4.73}Si_{7.27-7.70}O_{24}(Cl_{0.19-0.47}S_{0.00-0.25}C_{0.45-0.74})_{\Sigma 1.00}$. The chemical composition of scapolites mirrors the complex history and multistage evolution of the Evate deposit. The low-Cl, high-S scapolites from calc-silicate rocks are chemically indistinguishable from metamorphic scapolites, whereas the Cl-rich scapolite from carbonatite is interpreted as magmatic in origin. The gradual Cl enrichment reflects an increasing NaCl activity in the scapolite-forming fluid or melt. Both scapolite types are closely associated with amphibole and phlogopite, thus indicating amphibolite-facies conditions during retrograde stages of Late-Proterozoic (Ediacaran) granulite-facies metamorphism and/or Ordovician reactivation.

Key words: scapolite, Evate deposit, Mozambique

1. INTRODUCTION

Minerals of the scapolite supergroup are Cl-, C- or S -bearing tectosilicates with the general formula $M_4T_{12}O_{24}A$, where M = Na, Ca, K, T = Al, Si, and A = Cl, CO_3, SO_4. The anionic position A may also be occupied by minor OH^- and F^-. Ideal end-members compositions usually range between the marialite ($3NaAlSi_3O_8$, NaCl; *Ma*) and meionite ($3CaAl_2Si_2O_8$, $CaCO_3$; *Me*) end-members, resembling albite (*Ab*) and anorthite (*An*) compositions. However, meionite also forms a solid solution with silvialite ($3CaAl_2Si_2O_8$,$CaSO_4$) (Teertstra et al., 1999). "Mizzonite" is intermediate scapolite with a dominant marialite component. Naturally-occurring ideal end-member compositions are unknown, the majority of reported minerals range from Me_{20} to Me_{85} (Smith et al., 2008). The anionic composition reflects the environment of scapolite formation regarding Cl, CO_2, SO_3 and H_2O contents in fluids or melts.

The scapolite structure consists of two interpenetrating frameworks, $[(Si,Al)_{12}O_{24}]$ and $[Na,Ca][Cl,(CO_3)]$, with Al and Si cations distributed in different tetrahedral positions. Sodium and calcium cations rest in smaller cavities, whereas CO_3, SO_4, and Cl occur in larger cavities of the framework. The scapolite supergroup minerals crystallize with a tetragonal symmetry, in space groups $I4/m$ and $P4_2/n$, where the latter corresponds to the Me_{20-75} compositions with the highest degree of Al-Si order between the $T(2)$ and $T(3)$ sites (Hawthorne & Sokolova, 2008).

Scapolite crystallizes under silica-deficient magmatic, metamorphic and hydrothermal conditions. Scapolite has been found in alkali basalts (Boivin & Camus, 1981; Teertstra et al., 1999), diorites (Svenningsen, 1994; de Waal et al., 2002), alkali syenite (Brauns, 1914), latite (Goff et al., 1982), granitic pegmatite (Mittwede, 1994), veins in marble (Hogarth, 1970), pegmatoid veins in granulite (Blattner & Black, 1980), apatite-phlogopite-enstatite veins (Lieftink et al., 1993).

In regionally metamorphosed rocks, scapolite has been described from marble (Trommsdorff, 1966; Kerrick et al., 1973; Oterdoom, 1980; Sivaprakash, 1981; Frank, 1983; Schenk, 1984; Warren et al., 1987; Kusachi et al., 1999; Searle & Cox, 2002,), granulite (Rosen et al., 1977; Hoefs et al., 1981; Moecher et al., 1992; Abart et al., 2001; Madyukov et al., 2011; Porter & Austrheim, 2017; Hammerli et al., 2017), amphibolite (Ramsay & Davidson, 1970; Kassoli-Fournaraki, 1991; Raith & Högelsberger, 1994; Faryad, 2002; Pandit et al., 2003), and metagabbro (Jan & Karim, 1995; Yoshino & Satish-Kumar, 2001). Scapolites also occur in quartzite (Hietanen, 1967), metasediments (Mora and Valley, 1991), granitic and granodioritic plutons (Nabelek, 2002; Arranz et al., 2002), in contacts between granodiorite and biotite-gneiss (Mouchos et al., 2016), skarn dyke in limestone (Härme, 1965), zoned skarns at the contact with quartz monzonite (Shay, 1975), ilvaite-hedenbergite skarn (Mposkos, 1978), phlogopite-diopside-apatite skarn (Reznitsky, 1978), skarn associated with tungsten mineralization (Larsen, 1991), graphite-wollastonite-pyrrhotite skarns (Suzuki & Nakai, 1993), skarns at the contact of limestone and siltstone with calc-alkaline meta-aluminous dioritic gabbro (Franchini et al., 1999), two feldspar-scapolite-spessartine-romeite skarn (Christy & Gatedal, 2005), and iron-oxide-copper-gold ore deposits (Pan et al., 1994; Bernal et al., 2017).

Manuscript received 2019-06-24
Revised version accepted 2019-11-14

In metasomatic rocks, scapolite has been found as a pervasive replacement of plagioclase in gabbro and diorite (Vanko and Bishop, 1982), and in granite gneiss, amphibolites and metagabbros (Katongo et al., 2011), also in Cl-saturated metagabbro (Engvik et al., 2011), NaCl-rich scapolite pegmatite (Owen & Greenough, 1999), gabbroanorthosite changed by Cl-bearing fluid (Kullerud & Erambert, 1999).

Silvialite occurs in granulite-facies rocks and is also associated with mafic magmatic rocks (e.g., Boivin & Camus, 1981; Goff et al., 1982; Teertstra et al., 1999).

In southern Africa, scapolite is a relatively abundant metamorphic mineral in marbles, metagabbros, calc-silicate lithologies, granitic gneisses, and pelitic schists (Hanson et al., 1994; Katongo et al., 2011). Scapolite-rich layers in metasedimentary turbidite sequences of the Late Proterozoic – Early Paleozoic Damara Orogen (Behr et al., 1983; Swart, 1986; Schmidt-Mumm et al., 1987; Dombrowski et al., 1996) are interpreted as metamorphosed evaporites. Dense sulfate-rich brines accompanying the formation of Cu-Co, Ti, U and Au deposits of central and southern Africa were remobilized during metamorphism and percolated through basin sediments during late – to post-compressional deformations (Schmidt-Mumm et al., 1987; Saintilan et al., 2018).

Here, we describe scapolite from the Evate deposit of northeastern Mozambique to elucidate its origin. Geochronology of baddeleyite, zircon, zirconolite, U-rich thorianite, and monazite (Siegfried, 1999; Hurai et al., 2017, 2018) revealed polyphase Late Proterozoic to Late Ordovician evolution of the deposit. Since Cl and SO_4 contents of scapolite reflect activities of these anions in mineral-forming fluids (Orville, 1975; Ellis, 1978; Vanko & Bishop, 1982, Katongo et al., 2011), the scapolite chemistry may serve as a useful monitor of the fluid composition during various stages of the deposit formation.

2. GEOLOGICAL BACKGROUND

The Evate deposit (Fig. 1) occurs in the Monapo Klippe – an oval structure 40 × 35 km in size interpreted as a relict of a Neoproterozoic nappe metamorphosed under granulite-facies conditions (Pinna et al., 1993; Grantham et al., 2008; Viola et al., 2008) and pushed into the Mesoproterozoic basement of the Nampula Complex metamorphosed under amphibolite-facies conditions (Bingen et al., 2009; Macey et al., 2010). The Monapo Klippe consists of granulite-facies rocks of the Metachéria complex intruded by weakly metamorphosed, silica-oversaturated alkaline felsic rocks of the Ramiane suite and undersaturated alkaline mafic to ultramafic rocks of the Mazerapane suite.

The Evate deposit is an elongated body, about 3 km long and 850 m wide, consisting of 5 – 100 m thick apatite-magnetite-carbonate horizons intercalated with 2 – 40 m wide zones of

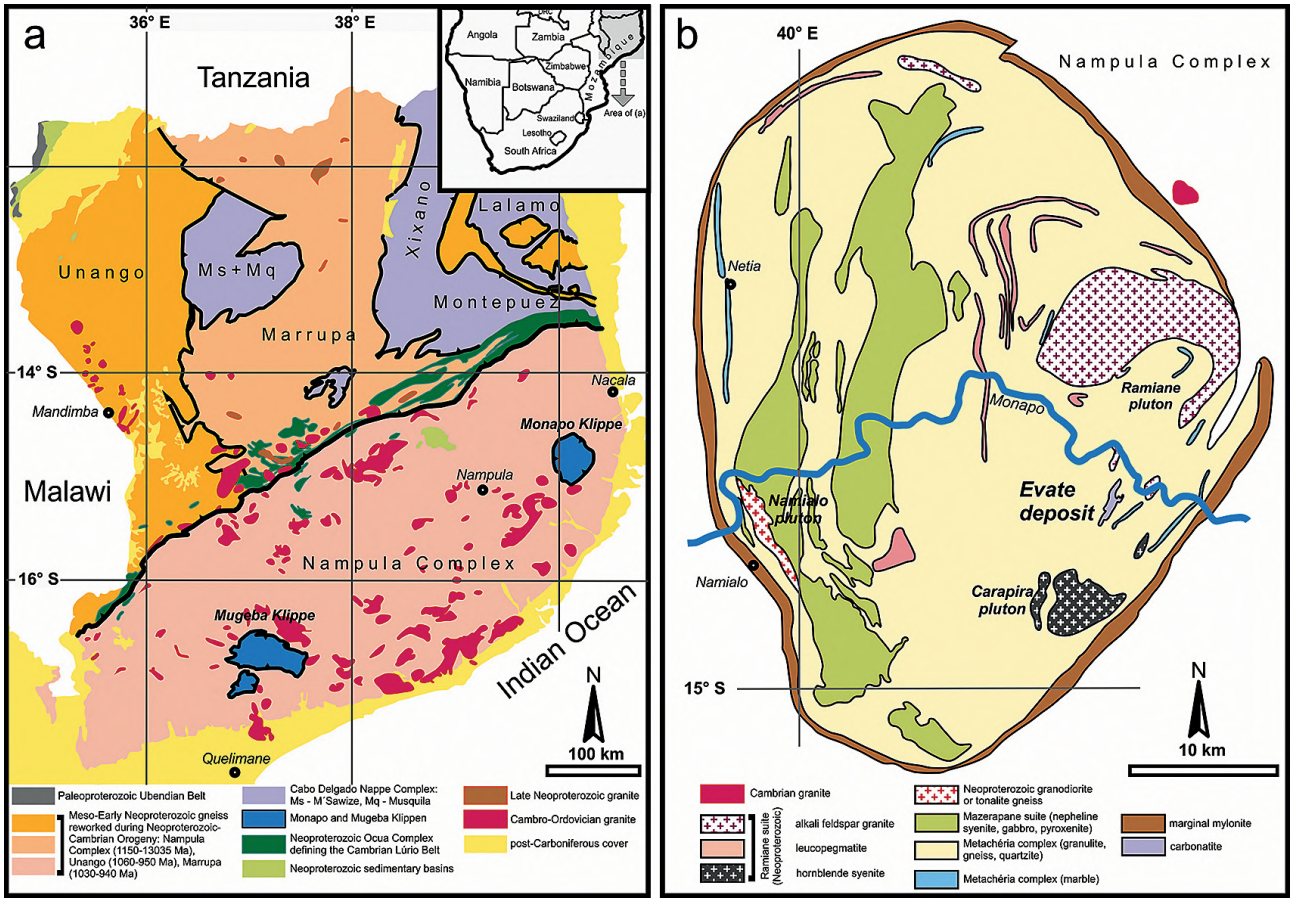

Fig. 1. Simplified geological maps of northern Mozambique (a) and Monapo Klippe (b) adapted from Macey et al. (2013).

biotite gneiss. Estimated resources correspond to ~ 155 Mt of apatite ores with an average P_2O_5 grade of 9.32 wt. % to a depth of 100 m (Geoindustria, 1982; Cílek, 1989). The deposit is covered with 3–38 m thick regolith containing 4–64 wt. % apatite (Davidson, 1986).

The genesis of the Evate deposit is contentious. A fenite aureole around apatite-magnetite-carbonate parts and close spatial relationship with surrounding felsic and mafic plutons has been interpreted as evidence of an intrusive magmatic origin (Macey et al., 2013; Barbosa et al., 2016). A hydrothermal-metasomatic origin has alternatively been proposed based on the preferential accumulation of apatite along N – S, W – E, and NW – SE-trending faults (Cílek, 1989). The deposit has also been described as a metasomatic/metamorphic marble (Karlsson, 2006; Ueda et al., 2012; Macey et al., 2013).

Uranium-Pb-(Th) dating of baddeleyite, zircon, zirconolite, U-rich thorianite, and monazite (Siegfried, 1999; Hurai et al., 2017, 2018) returned Late Proterozoic to Late Ordovician ages. The Late Ediacaran (~ 590 Ma) high-temperature (~ 800°C) phase was likely coincidental with post-granulite retrograde metamorphism. Mineral-forming processes ended with the precipitation of zeolites from low-temperature (< 300°C) alkaline carbo-hydrothermal fluids. Niobium-poor zirconolite and cerium-rich monazite yielded Late Ordovician ages (443 ± 3 and 449 ± 2 Ma). A Late Cambrian age of Nb-rich zirconolite (485 ± 9 Ma) and U-rich thorianite (493 ± 10 Ma) plotted between the age of Ce-rich monazite from anhydrite-bearing carbonatite and that of zircon and baddeleyite from magnetite-apatite-olivine rocks. The Early Palaeozoic evolution of the Evate deposit was driven by with the post-orogenic collapse and tectonic fragmentation of the Gondwana supercontinent (Hurai et al., 2018).

3. METHODS

The chemical composition of scapolites was measured using a CAMECA SX-100 electron probe (Geological Survey of Slovakia, Bratislava) operated in wavelength dispersive mode and the following analytical conditions: 15 kV accelerating voltage, 20 nA beam current, and beam diameter focused to 2 – 4 μm. The following standards, detector types and spectral lines were used: Si (orthoclase, TAP, Kα), Al (Al_2O_3, TAP, Kα), Ca (wollastonite, LPET, Kα), Ti (TiO_2, LPET, Kα), K (orthoclase, LPET, Kα), Na (albite, TAP, Kα), Mn (rhodonite, LLIF, Kα), Cr (Cr, LLIF, Kα), Mg (forsterite, TAP, Kα), Cl (NaCl, LPET, Kα), S (barite, LPET, Kα), Fe (fayalite, LLIF, Kα), Sr ($SrTiO_3$, LPET, Lα).

Scapolites contain 24 atoms of framework oxygen per formula unit (*apfu*). Hence, their formulae were calculated from electron probe microanalyses (EPMA) by normalizing to 12 Si + Al *apfu* (Teertstra and Sherriff, 1997). Monovalent and divalent cations were assigned to the *M* site. All Fe was taken as Fe^{2+}. The sum of cations in the *M* position was set to 4 *apfu*, whereas the sum of anions in the *A* position was normalized to 1 *apfu*. Carbon *apfu* values were calculated as C=1-Cl-F and then converted to CO_3 wt. % equivalent.

A confocal Xplora Raman spectrometer from Horiba Ltd. (Institute of Earth Sciences, Bratislava) was used for the characterization of vibration modes. The system includes a flat-field 20 cm spectrograph with a multichannel Peltier-cooled (– 70°C) Syncerity CCD detector (256 pixels) and a colour camera optically coupled to an Olympus BX-51 microscope. Raman spectra were collected with a 100× long-workingdistance objective lens (NA = 0.8, WD = 3.4 mm), 532 nm excitation wavelength of a 25 mW solid-state Nd-YAG laser, and 638 nm excitation wavelength of a 24 mW diode laser. A set of band-pass and edge filters were used to collect scattered light in the 100 – 4000 cm^{-1} region. The holographic grating with 1800 grooves/mm combined with a 50 μm entrance slit enabled the maximum spectral resolution of 0.4 cm^{-1} using the 532 nm excitation wavelength. The detector was calibrated by using the most intense vibrational band of silicon (520.7 cm^{-1}). Spectrum acquisition was done using the LabSpec6 software. Spectra were scanned first in real-time-display mode in various positions using the rotatable stage and then representative spectra were recorded using the 1800 grooves/mm spectrometer grating and 20 s acquisition time.

4. SAMPLES

Scapolites were identified in two drill cores obtained during the expedition of Geoindustria state enterprise in the early 1980s. Sample EVT-5 is calcite carbonatite from a depth of 170.4 m. The carbonatite is rimmed with a 2 cm thick band of amphibole crystals, separating it from a calc-silicate rock consisting of amphibole, biotite, and diopside (Fig. 2a). Massive homogeneous calcite in the carbonatite part is devoid of dolomite exsolutions. The amphibole-rich intermediate zone contains pargasite, actinolite, and hastingsite. Diopside with composition $Wo_{49-50}En_{44-45}Fs_{5-7}$ and biotite occur in the silicate-rich part. A massive aggregate of scapolite crystallized between the carbonatite and amphibole-rich parts (Figs. 2b-d). Scapolite contains paragonite inclusions and is associated with minor calcite, plagioclase (albite $Ab_{73-74}An_{25-27}Or_{0-1}$ to andesine $Ab_{51}An_{48}Or_1$), biotite, and allanite (Figs. 2e-f). Analcime replaces the scapolite along cleavage planes. Anhydrite and celestine occur as inclusions in calcite and as late infillings between adjacent calcite grains. Large apatite grains (Fig. 2f) in the scapolite-rich zone correspond to fluorapatite (2.3 – 2.9 wt. % F) with minor REE_2O_3 and SO_3 (0.3 – 0.4 wt. %). Allanite-(Ce) with variable REE contents (17.2 to 21.2 wt. %) forms thin rims around calcite and scapolite grains (Fig. 2e-f).

Sample F-70 is a calc-silicate rock from a depth of 109 m. Minerals identified using optical microscopy and EPMA comprise zoned amphiboles (hastingsite, hornblende, actinolite, and pargasite), diopside, phlogopite, allanite, epidote, apatite, K-feldspars, titanite, and minor calcite (Figs. 3a-d). Accessory apatite (Fig. 3a-b) corresponds to fluorapatite with a lower F (1.9 – 2.4 wt. %) and higher REE contents (0.5 – 0.8 wt. % REE_2O_3) relative to those in sample EVT-5. K-feldspar surrounded by phlogopite has a high Ba content (up to 11.4 wt. % BaO). Allanite forms large zoned grains with REE contents (10.2 – 19.6 wt. % REE_2O_3) dominated by Ce. Scapolite grains

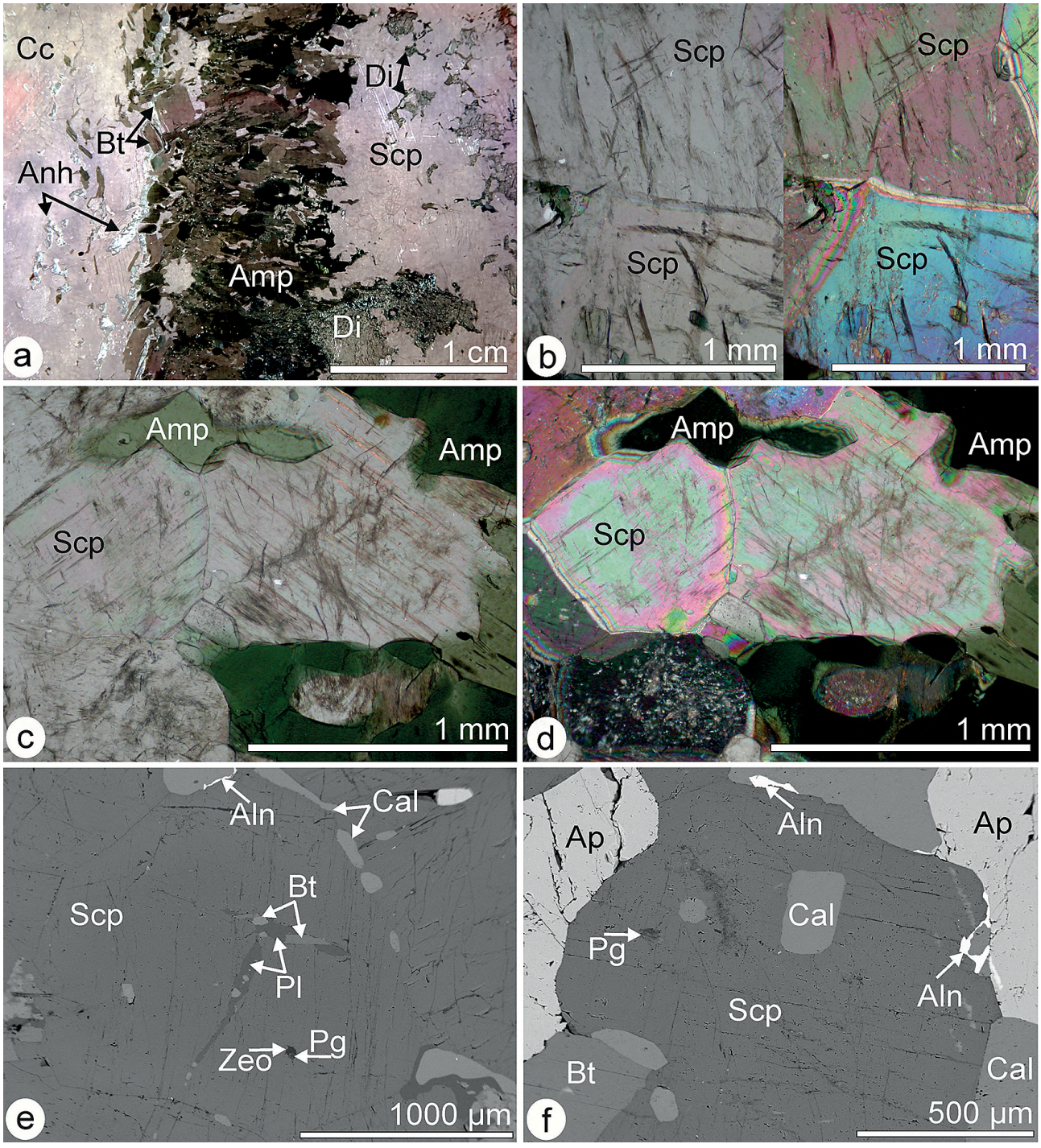

Fig. 2. Plane- and cross-polarized transmitted light images (a-d) and back-scattered electron images (e-f) of scapolite from carbonatite EVT-5. Mineral abbreviations refer to scapolite (Scp), amphibole (Amp), diopside (Di), biotite (Bt), anhydrite (Anh) and apatite (Ap). (e) Scapolite (Scp) associated with calcite (Cal), plagioclase (Pl), biotite (Bt), allanite (Aln) and zeolite (Zeo). (f) Scapolite associated with calcite, apatite, paragonite (Pg), biotite and late interstitial allanite.

interstitial to amphiboles and pyroxenes are transparent in transmitted plane-polarized light and show high relief and cleavage planes oriented in two directions. A dense network of minute pyrrhotite inclusions occur in scapolite cores (Fig. 3a,b). Only one larger sulfide aggregate within scapolite core, composed of pyrite, pyrrhotite, and chalcopyrite, 100-150 µm in size has been observed.

5. RESULTS

5.1 Raman spectrometry

Raman spectra of scapolite scanned in various grain orientations are shown in Fig. 4. Vibration spectra are largely similar for both investigated samples and include bands at 157, 255, 293, 414 – 418,

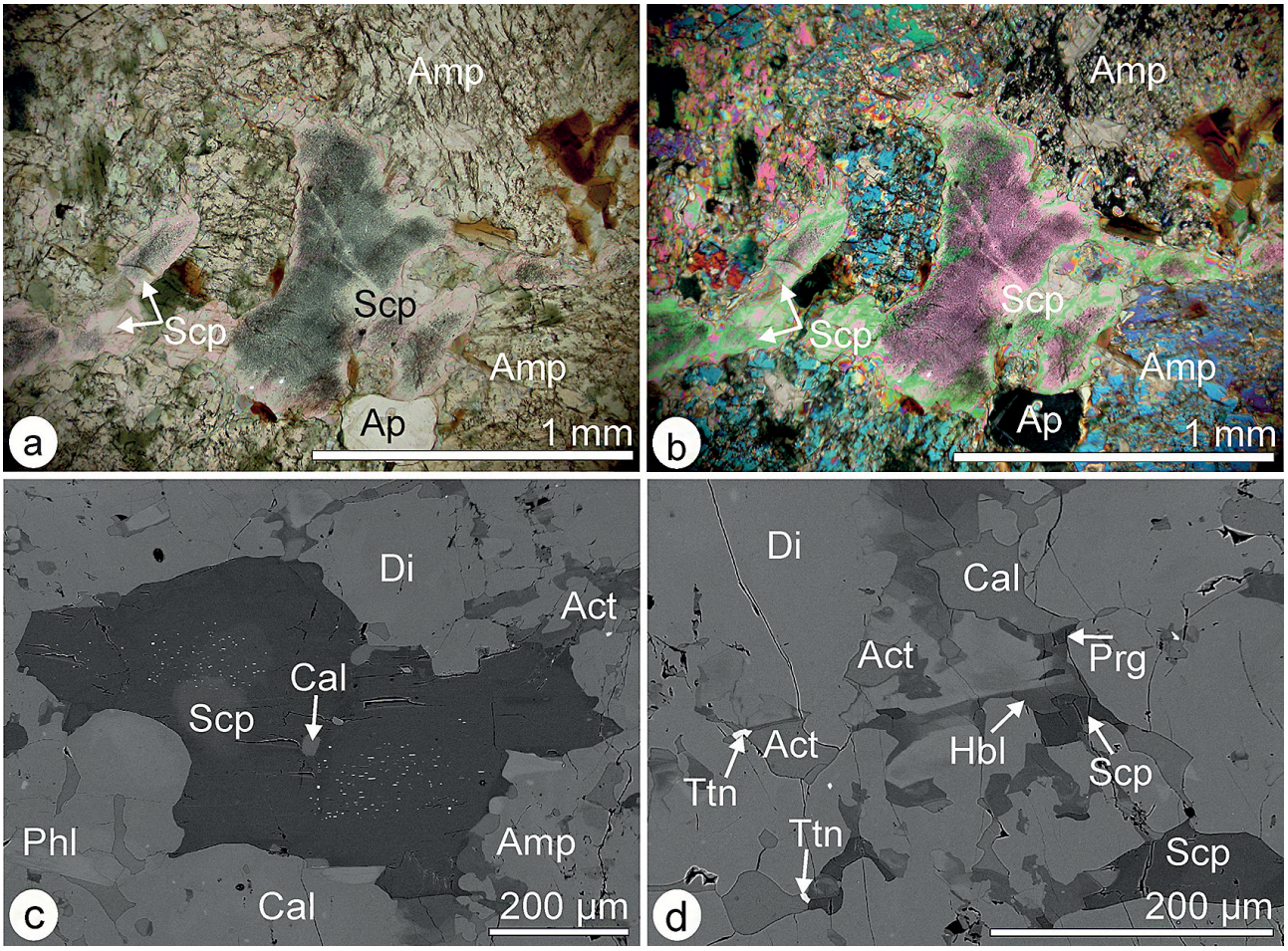

Fig. 3. Plane- and cross-polarized transmitted light images (**a-b**) and back-scattered electron images (**c-d**) of scapolite from calc-silicate drillcore F-70. Note gray-coloured scapolite cores in (**a**) and (**b**) with numerous Fe-sulphide (pyrrhotite) inclusions. (**c**) A large grain of scapolite with bright minute inclusions of pyrrhotite and an isolated calcite inclusion. Other minerals are represented by phlogopite (Phl), actinolite (Act), calcite and diopside (Di). (**d**) Scapolite associated with actinolite (Act), hornblende (Hbl), pargasite (Prg), diopside, calcite, and titanite (Ttn).

450, 527 – 534, 766 – 758, and 1094 – 1099 cm^{-1}, which are diagnostic of marialite and meionite (Lafuente et al., 2015). A strong band at 982 cm^{-1} in scapolite from calc-silicate sample F-70 is consistent with the main ν_1 vibration mode of the SO_4^{2-} ion (e.g., Schwarcz & Speelman, 1965). This band also occurs occasionally in other Cl-rich members of the scapolite supergroup (Lafuente et al., 2015) and could be attributed to the sulfate anion in the scapolite structure. Other anions could not be conclusively identified, as the main ν_1 vibration mode of CO_3^{2-} at ~ 1090 cm^{-1} is obscured by that of the SiO_4^{4-} group, and other CO_3^{2-} modes at 1400 – 1500 cm^{-1} together with the OH-stretching vibrations between 3000 and 4000 cm^{-1} were overwhelmed by strong fluorescence.

5.2 Chemical composition

Representative EPMA analyses are summarized in Tab. 1. Calcium (14.9 – 17.4 wt. % CaO) predominates over Na (3.2 – 4.9

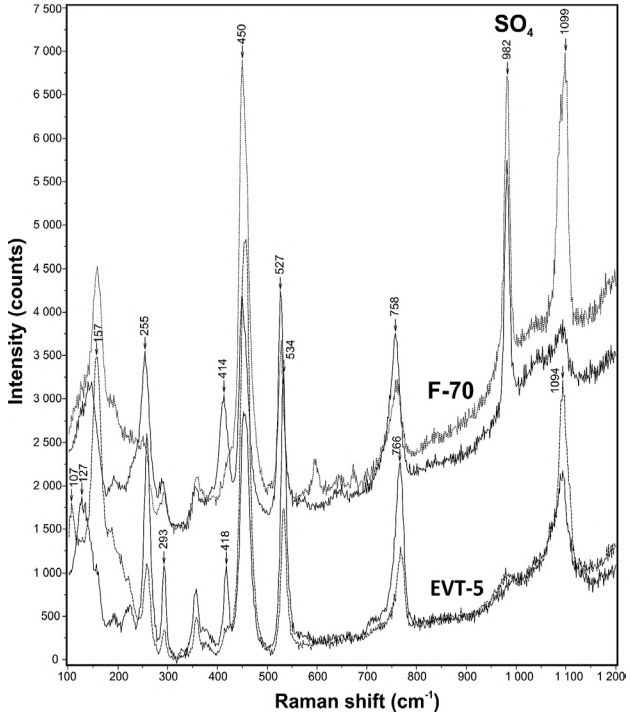

Fig. 4. Representative Raman spectra of scapolite grains from both samples scanned in two perpendicular orientations. Spectra are offset for clarity.

Tab. 1. Chemical composition of scapolites from Evate deposit with crystallochemical formulas based on 24 oxygen atoms, *T*-site occupancy (Si + Al) normalized to 12 cations and that of the *A*-site normalized to 1 anion. Fluorine content has been measured, but not detected.

Sample	F-70	F-70	F-70	F-70	F-70	EVT-5	EVT-5	EVT-5	EVT-5	EVT-5
No.	an1	an3	an5	an21	an1	an2	an4	an32	an9	an7
Type						I	I	I	II	II
SiO_2	45.54	47.17	47.68	45.30	44.95	50.71	51.72	51.71	48.63	50.46
Al_2O_3	26.94	26.11	25.04	26.77	26.89	25.5	24.49	24.61	25.46	25.27
FeO	0.03	0.13	0.08	0.05	0.04	0.02	0.02	0.01	0.01	0.15
CaO	16.78	15.97	14.78	16.99	17.21	12.91	11.79	11.48	14.45	13.21
SrO	1.06	0.84	0.78	0.96	0.92	0.42	0.31	0.29	0.49	0.49
Na_2O	3.62	4.31	4.92	3.54	3.33	6.25	7.00	7.02	5.27	6.34
K_2O	0.16	0.17	0.29	0.13	0.14	0.29	0.33	0.47	0.24	0.25
SO_4	2.45	2.35	1.86	2.21	2.34	0.04	0.02	0.50	2.71	1.83
CO_3*	3.37	3.33	3.23	3.55	3.51	3.03	2.75	2.41	2.56	2.59
Cl	0.33	0.41	0.66	0.28	0.26	1.53	1.77	1.86	0.88	1.23
O=Cl	0.07	0.09	0.15	0.06	0.06	0.35	0.40	0.42	0.20	0.27
Total	**100.21**	**100.7**	**99.17**	**99.72**	**99.53**	**100.35**	**100.52**	**99.94**	**100.5**	**101.55**
Si	7.07	7.26	7.37	7.07	7.04	7.59	7.70	7.69	7.42	7.55
Al	4.93	4.74	4.63	4.93	4.96	4.41	4.30	4.31	4.58	4.45
Σ T	**12.00**	**12.00**	**12.00**	**12.00**	**12.00**	**12.00**	**12.00**	**12.00**	**12.00**	**12.00**
Fe^{2+}	0.00	0.02	0.01	0.00	0.00	0.00	0.00	0.00	0.00	0.02
Ca	2.79	2.63	2.43	2.84	2.89	2.07	1.88	1.83	2.36	02.11
Sr	0.09	0.07	0.07	0.08	0.08	0.04	0.03	0.02	0.04	0.04
Na	1.09	1.29	1.47	1.07	1.01	1.81	2.02	2.07	1.56	1.83
K	0.03	0.03	0.05	0.03	0.03	0.06	0.06	0.09	0.05	0.05
Σ M	**4.00**	**4.04**	**4.03**	**4.02**	**4.01**	**3.98**	**3.99**	**4.01**	**4.01**	**4.05**
S	0.24	0.23	0.18	0.22	0.23	0.00	0.00	0.04	0.26	0.17
C	0.67	0.66	0.65	0.71	0.70	0.61	0.55	0.49	0.51	0.52
Cl	0.09	0.11	0.17	0.07	0.07	0.39	0.45	0.47	0.23	0.31
Σ A	**1.00**	**1.00**	**1.00**	**1.00**	**1.00**	**1.00**	**1.00**	**1.00**	**1.00**	**1.00**
Σ	16.00	16.04	16.03	16.02	16.01	15.98	15.99	16.01	16.01	16.05
Me%**	72	67	63	73	74	53	48	47	60	54
Ma%**	28	33	37	27	26	47	53	53	40	46
Eq_{An}**	64	58	54	65	65	47	43	44	53	48

*CO_3 calculated as C = 1-S-Cl and converted to oxide wt. %

** Marialite *Ma* =100 (Na/[Na+Ca+K]) and meionite *Me* = 100(Ca/[Ca+Na+K]) components in mole % (Shaw, 1960), Eq_{An} is an equivalent anorthite component in mole % calculated as Eq_{An} = 100(Al-3)/3 (Evans et al., 1969).

wt. % Na_2O) in calc-silicate sample F-70, whereas slightly lower CaO and higher Na_2O contents (11.5 – 15.4 and 4.9 – 7.2 wt. %, respectively) were recorded in carbonatite EVT-5. Strontium is present in minor quantities (0.3 – 1.2 wt. % SrO). The two samples also differ in the occupancy of their anionic positions. The Cl content is in the range of 0.2 – 0.7 wt. % and the SO_4 content fluctuates from 1.8 to 2.6 wt. % in calc-silicate F-70. In contrast, scapolite from carbonatite EVT-5 shows higher Cl values (0.8 – 1.9 wt. %) and a wider SO_4 range (nil to 2.7 wt. %). Calculated CO_3 contents are generally higher in F-70 (3.2 – 3.6 wt. %) compared to EVT-5 (2.3 – 3.7 wt. %).

Apart from the proportion of marialite and meionite components, the scapolite nomenclature also relies on the equivalent anorthite component (Eq_{An} = 100(Al – 3)/3) often used for comparison with plagioclases (Evans et al., 1969). For the range of Ca/(Ca + Na) ratios from 0 to 0.75, the scapolite compositions change linearly between ideal marialite end-member $Na_4Al_3Si_9O_{24}Cl$ (*Ma*) and $NaCa_3Al_5Si_7O_{24}CO_3$ component through the substitution of Na_3Si_2Cl with $Ca_3Al_2CO_3$ (Ca can be substituted by minor Sr, Na by K, and CO_3 by SO_4). For the Ca/(Ca + Na) range between 0.75 and 1, the compositions between $Na_4Al_3Si_9O_{24}Cl$ and $Ca_4Al_5Si_7O_{24}CO_3$ end-members are obtained by replacing the NaSi component with CaAl as in plagioclases, without the change in the anionic site fully occupied at 0.75 *apfu* (Evans et al., 1969).

Early scapolite from carbonatite EVT-5 is depleted in sulphur (nil to 0.05 *apfu*), particularly in grain centers associated with biotite. The scapolite rims are significantly enriched in S (0.15 – 0.26 *apfu*), particularly along grain margins in contact with apatite, calcite, and allanite. Scapolites from carbonatite EVT-5 exhibit Eq_{An} values between 43 and 58, whereas marialite and meionite contents are almost similar (46 – 63 mol. % *Me*). These scapolites contain lower Ca (1.82 – 2.49 *apfu*), higher Na (1.44 – 2.07 *apfu*), Cl (0.19 – 0.47 *apfu*) and calculated C contents (0.45 – 0.74 *apfu*)

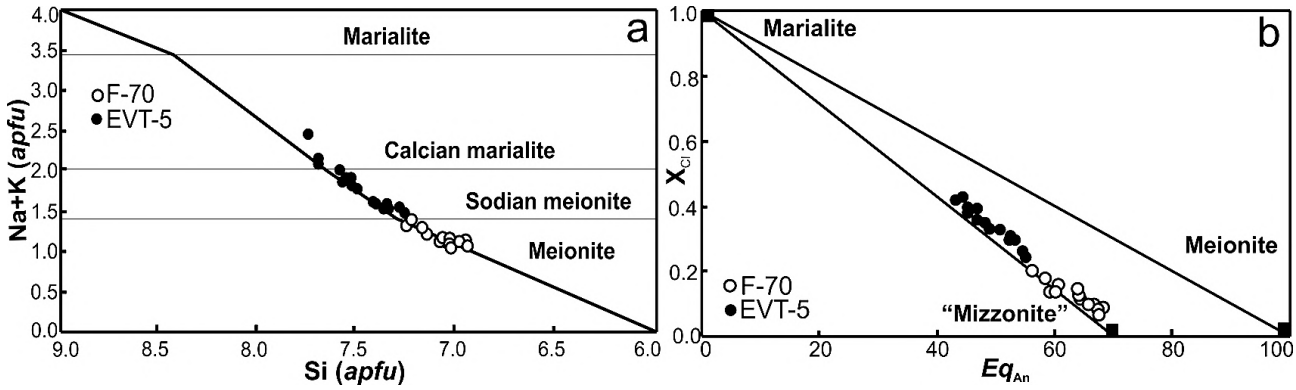

Fig. 5. a) Diagram (Na + K) *versus* Si (*apfu*) shows scapolite end-members (marialite and meionite) according to the nomenclature of Teertstra et al. (1999) based on structural changes. Labels of minerals are as follows: Me_{0-15} marialite, Me_{15-50} calcian marialite, Me_{50-65} sodic meionite, and Me_{65-100} meionite. b) Chemical composition of scapolite in the Eq_{An} *versus* X_{Cl} diagram with meionite, marialite end-members, and "mizzonite" denoted by black squares (modified after Evans et al., 1969). "Mizzonite" is intermediate scapolite with $Eq_{An} \approx 0.75$.

in comparison with sample F-70. The composition of EVT-5 scapolite expressed as formula is $(Na_{1.43-2.07}Ca_{1.82-2.50})_{\Sigma 3.97-4.11}Al_{4.29-4.73}Si_{7.27-7.70}O_{24}(Cl_{0.19-0.47}S_{0.00-0.25}C_{0.45-0.74})_{\Sigma 1.00}$.

Scapolites from calc-silicate rock F-70 exhibit higher Eq_{An} values (54 – 68 mol. %), higher Ca and meionite contents (2.46 – 2.99 *apfu* and 62 – 74 mol. %, respectively), but lower Na and Cl values (1.0 – 1.47 *apfu* and 0.06 – 0.17 *apfu*), respectively, and calculated C contents within the range of 0.64 – 0.71 *apfu*. Their formula is $(Ca_{2.46-2.99}Na_{1.00-1.47})_{\Sigma 4.00-4.20}Al_{4.62-5.04}Si_{6.95-7.37}O_{24}(Cl_{0.06-0.17}S_{0.18-0.26}C_{0.64-0.70})_{\Sigma 1.00}$. All scapolites from Evate plot along the marialite-"mizzonite" (intermediate scapolite with EqAn ≈ 0.75) join (Fig. 5), thus reflecting the dominant solid solution between Cl^- and CO_3^{2-} end-members, and subordinate substitution between the Cl^- and SO_4^{2-} end-members. All scapolites fall into the group of sodic scapolites with the maximal Al-Si order between the $T(2)$ and $T(3)$ sites, thus probably corresponding to the $P4_2/n$ space group (Hawthorne & Sokolova, 2008). Few analyses from carbonatite EVT-5 plot within the field of calcic marialite. The scapolite from calc-silicate drillcore F-70 is more meionitic (Ca-rich) compared with that from EVT-5 (Figs. 6 – 7).

6. DISCUSSION

The dominant Cl- and CO_3–rich end-member substitution in scapolites from Evate is illustrated in Fig. 8a, which also summarizes data on scapolites of various origins. Scapolites from calc-silicate drillcore F-70 overlap the field of scapolites from metamorphosed calc-silicate rocks aligned along the meionite-silvialite join. Compositionally similar scapolites from Sludyanka (Russia) are also attributed to a metamorphogenic origin (Reznitsky, 1978).

Scapolites with different SO_4 / [SO_4 + CO_3 + Cl] ratios have been distinguished in the carbonatite drillcore EVT-5. The earliest generation of scapolite to crystallize (Scp I, Fig. 8a) has relatively low SO_4 / [SO_4 + CO_3 + Cl] ratios and high Cl content and is similar to scapolite from alkali-basaltic Kula Volcanic Province in Turkey (Smith et al., 2008). A younger generation (Scp II) has higher SO_4 / [SO_4 + CO_3 + Cl] ratios and is similar to scapolite from pegmatite associated with carbonatites from Ilmeny Mountains in Russia (Korinevsky, 2015; Korinevsky & Korinevsky, 2016). Both scapolite types plot within the field of magmatic scapolite. The magmatic

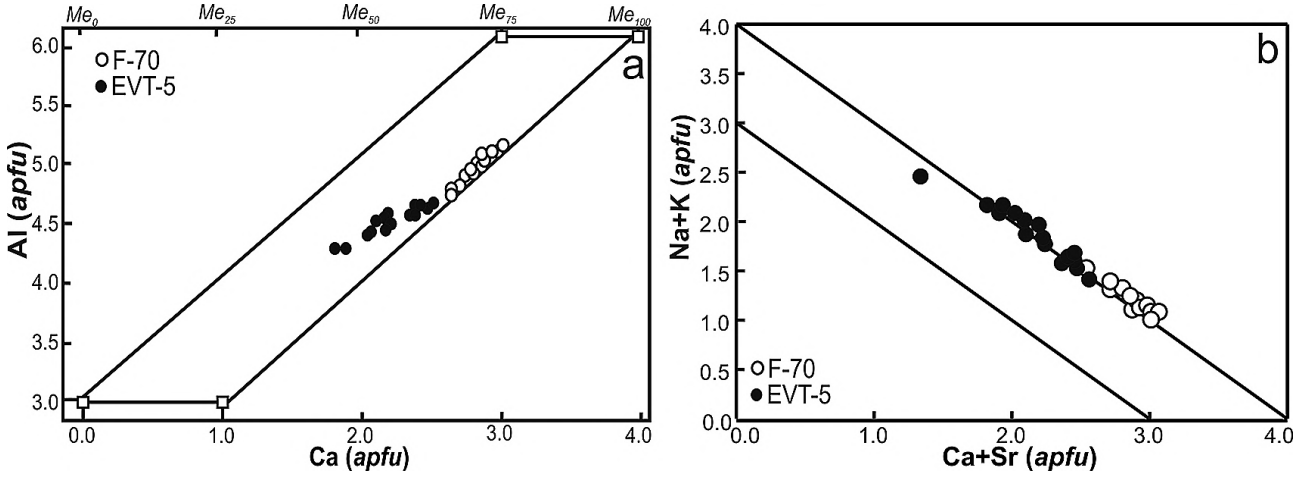

Fig. 6. a) Compositional plot of scapolites modified after Hawthorne and Sokolova (2008). Open squares correspond to end-member compositions. b) Plot of (Na + K) *versus* (Ca + Sr) (*apfu*) with iso-lines for Σ*M* = 3 and 4 *apfu* (modified after Teertstra et al. 1999).

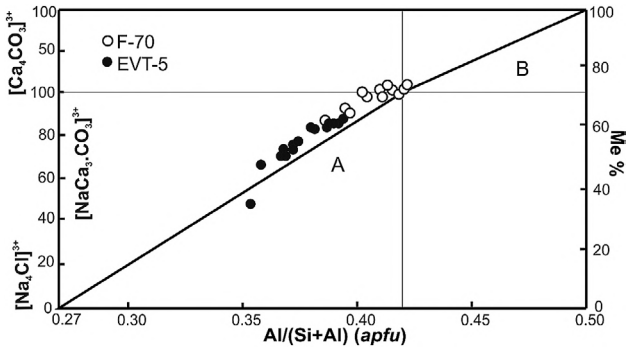

Fig. 7. Plot of Al / (Al + Si) (*apfu*) versus the percentage of meionite component and end-member fractions modified after Hassan and Buseck (1988). The solid line denotes the substitution of $[Na_4Cl]Si_2$ by $[NaCa_3CO_3]Al_2$ in series A and the substitution of $[NaCa_3CO_3]Si$ by $[Ca_4CO_3]Al$ in series B. Series A also represents sodic scapolite, whereas series B represents calcic scapolite. The two substitutional mechanisms operate independently.

origin of the Evate deposit is also corroborated by the presence of molybdenite and high crystalliztion temperatures, > 814 °C derived from the calcite-dolomite thermometry (Hurai et al. 2017).

Primary magmatic scapolite is not common, but it has been reported to crystallize from silica-deficient magmas enriched in CO_2, SO_3, and/or Cl (Goff et al., 1982). As a rule, the magmatic scapolites are more meionitic (Ca-rich) in composition. Such compositions indicate relatively high CO_2 partial pressure, and high temperatures and pressures, exceeding 850 °C (Goldsmith & Newton, 1977; Millhollen, 1974; Goff et al., 1982; Oterdoom & Wenk, 1983; Smith et al., 2008) and 3 kbar (Millhollen, 1974; Smith et al., 2008), respectively. Compositions approaching pure meionite endmembers have not been observed in magmatic rocks.

Meionitic scapolite is also typical of calc-silicate rocks metamorphosed under amphibolite- and granulite-facies conditions (Fig. 8a). Scapolite analyses from these rocks span from the CO_3-apex, corresponding to the CO_3 content of ~ 4 – 5 wt. %, towards the SO_4-apex, reaching SO_4 values as high as 7 wt. % SO_4, corresponding to the SO_4 / $[SO_4 + CO_3 + Cl]$ ratio of 0.82 (Schenk, 1984). Sulphur-rich scapolite also crystallizes at elevated temperatures, approaching 90 – 1000 °C (Goldsmith & Newton, 1977), and/or under high partial pressures of SO_3 in the coexisting fluid (Goff et al., 1982). Although granulite facies rocks are often considered volatile-free rocks, granulite-hosted silvialite provides a sulphate reservoir, which becomes unstable during retrograde hydration under amphibolite-facies conditions (Goldsmith & Newton, 1977; Schenk, 1984).

Scapolite from calc-silicate drillcore sample F-70 with the maximum SO_4 / $[SO_4 + CO_3 + Cl]$ value of 0.38 plots in between the SO_4- and CO_3-rich end-members typical of granulite-facies rocks. The high sulphate content in the scapolite was corroborated by the intense Raman vibration at 982 cm^{-1}. The presence of actinolite, hornblende, and pargasite (Figs. 2 and 3) indicates amphibolite-facies conditions.

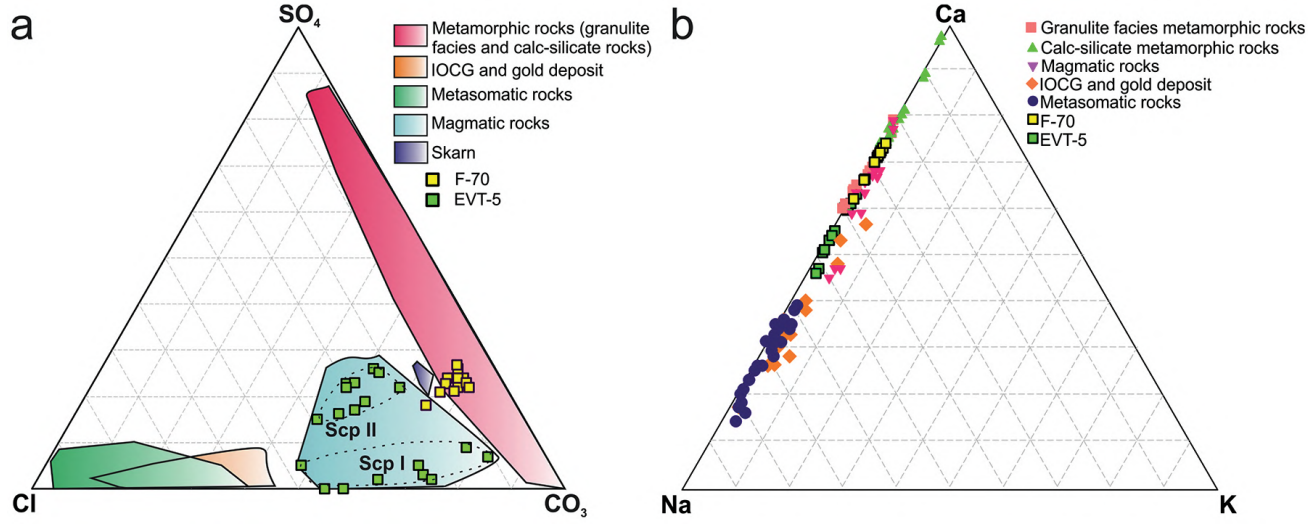

Fig. 8. a) SO_4-Cl-CO_3 diagram for the scapolite supergroup with analytical data from Evate and compositional fields for various genetic types of scapolites compiled from literature: *metamorphic rocks*: granulite facies – Bergen Arcs, Norway (Porter and Austrheim, 2017); Massif Central, France, New South Wales, Australia, Shai Hill, Ghana (Hammerli et al., 2017); calc-silicate rocks – Sare Sang, Afghanistan (Faryad, 2002); Kerala Khondalite Belt, India (Satish-Kumar and Harley, 1998); Takab, Iran (Moazzen et al., 2009); Central Alps, Switzerland (Kuhn et al., 2005); Maligawila, Sri Lanka (Mathavan and Fernando, 2001); Sarti, Greece (Kassoli-Fournaraki, 1991); Ghats Belt, India (Dasgupta and Pal, 2005); Pamir, Tajikistan (Madyukov et al., 2011); Sludyanka, Russia (Reznitsky, 1978). *Skarn* – Långban, Värmland, Sweden (Christy and Gathedal, 2005). *IOCG and gold deposits* – Norrbotten County, Sweden (Bernal et al., 2017); Nickel Plate and Hemlo, Canada (Pan et al., 1994). *Metasomatic rocks* – Humboldt igneuos lopolith, Nevada, USA (Vanko and Bishop, 1982); Nusfjord, Lofoten, Norway (Kullerud and Erambert, 1999); Ødegårdens Verk, Bamble, Norway (Lieftink et al., 1993; Engvik et al., 2011); Idaho, USA (Mora and Valley, 1991); Lufilian–Zambezi Belt, Zambia (Katongo et al., 2011); Minas fault, Nova Scotia, Canada (Owen and Greenough, 1999); Sudbury, Ontario, Canada (Schandl et al., 2011). *Magmatic rocks* – scapolite megacryst in alkali basalt, Olot Suite, Spain (Torró et al., 2018); cumulate nodules, Kula Volcanic Province, Turkey (Smith et al., 2008); pegmatite associated with carbonatites, Ilmeny Mountains, Russia (Korinevsky, 2015; Korinevsky and Korinevsky, 2016); gem-quality scapolite, Ihosy, Madagascar (Superchi et al., 2010). b) Ca-Na-K diagram of scapolites from different rock types. Note that all scapolites are poor in K and substitution exists only between the Ca- and Na-dominant end-members.

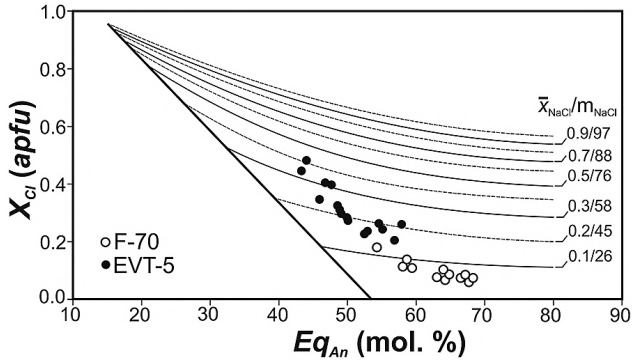

Fig. 9. Salinities of aqueous fluids coexisting with scapolite of the marialite-meionite series (Ellis, 1978) superimposed on the X_{Cl} versus Eq_{An} diagram expressing the scapolite composition (modified after Evans et al., 1969). Concentration units along isopleths (subhorizontal dashed and solid curves) refer to mole fraction (x_{NaCl}) and mass percentage (m_{NaCl} in wt. %) of NaCl in the coexisting aqueous fluid.

According to the experiments with scapolite solid solutions at 750 °C and 4 kbar (Orville, 1975) almost pure marialite end-member occurs in rocks with high NaCl activity. Therefore scapolites in metasomatic rocks have high Cl content (green area in Fig. 8a). These scapolites are mostly formed by pervasive replacement of plagioclase (Vanko & Bishop, 1982; Katongo et al., 2011), and are predominantly marialitic in composition. Scapolite in IOCG deposit in Norrbotten County is also *Ma*-rich with halogen signature related to seawater, magmatic and evaporitic sources (Bernal et al., 2017).

The Ca-Na-K substitution at cation position (Fig. 8b) is observed only between Ca and Na. K content in scapolites from all rock types is very low. Magmatic scapolite from EVT-5 sample plots between Ca and Na with intermediate composition, similar to anionic positions in SO_4-Cl-CO_3 diagram (Fig. 8a). Scapolites from calc-silicate rock F-70 have higher Ca content (Me-rich) and plot close to Ca-apex together with rocks with similar composition. Metasomatically altered rocks are Ma-rich with increased Na content.

The scapolite composition plotted against the isopleths of coexisting aqueous fluids (Fig. 9) indicates salinities lower than 26 wt. % NaCl in the calc-silicate sample F-70 contrasting with salinities from 36 up to 68 wt. % associated with the carbonatite drillcore EVT-5. It must be emphasized, however, that the diagram was constructed for temperatures and pressures of 750 °C and 4 kbar, respectively. Projection points of Ca-rich marialite (28 – 46 % *Me*, X_{Cl} = 0.37 – 0.84) from metagabbros and amphibolites of the Lufilian-Zambezi belt affiliated with the amphibolite-facies metamorphism plot in the same diagram at higher or even unrealistically high NaCl concentrations, exceeding the X_{NaCl} value of pure NaCl (Katongo et al., 2011).

7. CONCLUSION

Two scapolite types have been distinguished in the apatite-carbonatite deposit of Evate in NE Mozambique. The Cl-rich scapolite from carbonatite projects within the field of magmatic scapolites, thus providing a piece of additional evidence for the magmatic stage involved in the history of the Evate deposit. In contrast, Cl-poor and S-rich scapolite with pyrrhotite inclusions from calc-silicate rock projects within the field of metamorphic scapolites. An intimate spatial relationship of both scapolite types with actinolitic and pargasitic amphiboles indicates amphibolite-facies conditions. Contrasting Cl contents reflect different NaCl activities in the coexisting fluid or melt.

Acknowledgements: This study was supported by the VEGA grant No. 2/0118/16 and the Centre of Excellence for Integrated Research on the Geosphere (ITMS 26220120064) funded by the Research and Development Operation Program. The initial version of the manuscript strongly benefited from constructive reviews of A. R. Chakhmouradian and an anonymous reviewer.

References

Abart R., Schmud R. & Harlov D., 2001: Metasomatic coronas around hornblendite xenoliths in granulite facies marble, Ivrea Zone, N Italy: I. Constraints on component mobility. *Contributions to Mineralogy and Petrology*, 141, 473–493.

Arranz E., Lago M., Bastida J. & Gale C., 2002: Hydrothermal scapolite related to the contact metamorphism of the Maladeta Plutonic Complex, Pyrenees: chemistry and genetic mechanisms. *Schweizerische Mineralogische und Petrographische Mitteilungen*, 82, 101–119.

Barbosa R.O., Masotti F.S., Etchart E.F., Mabota N., Gaspar J.C. & Júnior E.F., 2016: Geological characterization of the Evate carbonatite. *In:* 35th International Geological Congress, Cape Town, S. Africa, Abstracts, Paper Number 613.

Behr H.J., Ahrendt H., Porada H., Röhrs J. & Weber K., 1983: Upper Proterozoic playa and sabkha deposits in the Damara orogen, SWA/Namibia. *In:* R.M.G. Miller (Ed.), Evolution of the Damara Orogen of southwest Africa/Namibia. *Special Publication Geological Society of South Africa*, 11, 1–20.

Bernal N.F., Gleeson S.A., Smith M.P., Barnes J.D. & Pan Y., 2017: Evidence of multiple halogen sources in scapolites from iron oxide-copper-gold (IOCG) deposits and regional Na-Cl metasomatic alteration, Norrbotten County, Sweden. *Chemical Geology*, 451, 90–103.

Bingen B., Jacobs J., Viola G., Henderson I.H.C., Skar Ø., Boyd R., Thomas R.J., Solli A., Key R.M. & Daudi E.X.F., 2009: Geochronology of the Precambrian crust in the Mozambique belt in NE Mozambique, and implications for Gondwana assembly. *Precambrian Research*, 170, 231–255.

Blattner P. & Black P.M., 1980: Apatite and scapolite as petrogenetic indicators in granulites of Miford Sound, New Zealand. *Contributions to Mineralogy and Petrology*, 74, 339–348.

Boivin P. & Camus G., 1981: Igneous scapolite-bearing associations in the Chaîne des Puys, Massif Central (France) and Atakor (Hoggar, Algeria). *Contributions to Mineralogy and Petrology*, 77, 365–375.

Brauns R., 1914: Skapolithführende Auswürflinge aus dem Laacher Seegebiet. *Neues Jahrbuch für Geologie und Paläontologie*, 39, 79–125.

Christy A.G. & Gatedal K., 2005: Extremely Pb-rich rock-forming silicates including a beryllian scapolite and associated minerals in a skarn from Långban, Värmland, Sweden. *Mineralogical Magazine*, 69, 995–1018.

Cílek V., 1989: Industrial Minerals of Mozambique. Czech Geological Office, Praha, 334 p. (ISBN 80-7075-027-8).

Dasgupta S. & Pal S., 2005: Origin of grandite garnet in calc-silicate granulites: mineral–fluid equilibria and petrogenetic grids. *Journal of Petrology*, 46, 1045–1076.

Davidson D.F., 1986: Phosphate Resources of Mozambique Based on Available Data. In: Final Report to UN/DTCD, INT/80-R45. United Nations, New York.

de Waal S.A., Graham I.T. & Phillips D., 2002: Age and significance of the Marble Hall breccia, Bushveld Complex, South Africa. *South African Journal of Geology*, 105, 227–240.

Dombrowski A., Hoernes S. & Okrusch M., 1996: Scapolitization in the Kuiseb Formation of the Damara Orogen: geochemical and stable isotope evidence for fluid infiltration along deep crustal shear zones. *Communications of the Geological Survey of Namibia*, 11, 13–31.

Ellis D.M., 1978: Stability and phase equilibria of chloride- and carbonate-bearing scapolites at 750 °C and 4000 bar. *Geochimica et Cosmochimica Acta*, 42, 1271–1281.

Engvik A. K., Mezger K., Wortelkamp S., Bast R., Corfu F., Korneliussen A., Ihlen P., Bingen B. & Austrheim H., 2011: Metasomatism of gabbro – mineral replacement and element mobilization during the Sveconorwegian metamorphic event. *Journal of Metamorphic Geology*, 29, 399–423.

Evans B.W., Shaw D.M. & Haughton D.R., 1969: Scapolite stoichiometry. *Contributions to Mineralogy and Petrology*, 24, 293–305.

Faryad S.W., 2002: Metamorphic conditions and fluid compositions of scapolite bearing rocks from the lapis lazuli deposit at Sare Sang, Afghanistan. *Journal of Petrology*, 4, 725–747.

Franchini M.B., Meinert L.D. & Schalamuck A.J., 1999: Mineralized scapolite-rich skarns from Cajón Grande and Cajón Medio creeks, NW Neuquén, Agrentina. *Mineral Deposits: Processes to Processing.* Balkema, Rotterdam, pp. 1043–1046.

Frank E., 1983: Alpine metamorphism of calcareous rocks along a cross-section in the Central Alps: occurrence and breakdown of muscovite, margarite and paragonite. *Schweizerische Mineralogische und Petrographische Mitteilungen*, 63, 37–93.

Geoindustria, 1982: Project of geological exploration I. Geological prospection of apatite- titanomagnetite deposits in the region of Evate. In: Regional Prospection of the Annular Monapo Structure. Open File report, Geoindustria, Praha, 1-133.

Goff F., Arney B.H. & Eddy A.C., 1982: Scapolite phenocrysts in a latite dome, northwest Arizona, U.S A. *Earth and Planetary Science Letters*, 60, 86–92.

Goldsmith J.R. & Newton R.C., 1977: Scapolite plagioclase stability relations at highpressures and temperatures in system $NaAlSi_3O_8$-$CaAl_2Si_2O_8$-$CaCO_3$-$CaSO_4$. *American Mineralogist*, 62, 1063–1081.

Grantham G.H., Macey P.H., Ingram B.A., Roberts M.P., Armstrong R.A., Hokada T., Shiraishi K., Jackson C., Bisnath A. & Manhiça V., 2008: Terrane correlation between Antarctica, Mozambique and Sri Lanka: comparison of geochronology, lithology, structure and metamorphism and possible implications for the geology of southern Africa and Antarctica. *In:* Satish-Kumar M., Motoyoshi Y., Osanai Y., Hiroi Y. & Siraishi K. (Eds.): Geodynamic evolution of East Antarctica: a key to the EastWest Gondwana connection. *Geological Society London Special Publications*, 308, 91–119.

Hammerli J., Kemp A.I.S., Barrett N., Wing B.A, Roberts M., Arculus R.J., Boivin P., Nude P.M. & Rankenburg K., 2017: Sulfur isotope signatures in the lower crust: A SIMS study on S-rich scapolite of granulites. *Chemical Geology*, 454, 54–66.

Hanson R.E., Wilson T.J. & Munjanyiwa H., 1994: Geologic evolution of the Neoproterozoic Zambezi orogenic belt in Zambia. *Journal of African Earth Sciences*, 18, 135–150.

Härme M., 1965: A zoned skarn dike in Silvola, southern Finland. *Bulletin of the Geological Society of Finland*, 218 (C. R. Soc. Geol. Finlande, 37), 99–106.

Hassan I. & Buseck P.R., 1988: HRTEM characterization of scapolite solid solutions. *American Mineralogist*, 73, 119–134.

Hawthorne F. C. & Sokolova E., 2008: The crystal chemistry of the scapolite-group minerals. II. The origin of the $I4/m \leftrightarrow P4_2/n$ phase transition and the nonlinear variations in chemical composition. *Canadian Mineralogist*, 46, 1555–1575.

Hietanen A., 1967: Scapolite in the Belt Series in the St. Joe-Clearwater Region, Idaho. *Geology Society of America Special Papers*, 86, 1–54. DOI:10.1130/spe86-p1.

Hoefs J., Coolen J.J.M. & Touret J., 1981: The sulfur and carbon isotope composition of scapolite-rich granulites from southern Tanzania. *Contribution to Mineralogy and Petrology*, 78, 332–336.

Hogarth D.D., 1970: Mineral occurence in the western Lake Baikal district, U.S.S.R. *Mineralogical Record*, 1, 58–64.

Hurai V., Huraiová M., Gajdošová M., Konečný P., Slobodník M. & Siegfried P.R., 2018: Compositional variations of zirconolite from the Evate apatite deposit (Mozambique) as an indicator of magmatic-hydrothermal conditions during postorogenic collapse of Gondwana. *Mineralogy and Petrology*, 112, 279–296.

Hurai V., Paquette J.L., Huraiová M., Slobodník M., Hvožďara P., Siegfried P.R., Gajdošová M. & Milovská S., 2017. New insights into the origin of the Evate apatite iron oxide-carbonate deposit, Northeastern Mozambique, constrained by mineralogy, textures, thermochronometry, and fluid inclusions. *Ore Geology Reviews*, 80, 1072–1091.

Jan M.Q. & Karim A., 1995: Coronas and high-P veins in metagabbros of the Kohistan island arc, northern Pakistan: evidence of crustal thickening during cooling. *Journal of Metamorphic Geology*, 13, 357–366.

Karlsson J.P., 2006: An investigation of the felsic Ramiane Pluton in the Monapo structure, Northern Mocambique. Examensarbeten I Geologi vid Lunds Universitet – Berggrundsgeologi 202.

Kassoli-Fournaraki A., 1991: Ca-rich scapolite in quartz amphibolites from the Sarti area, northern Greece. *European Journal of Mineralogy*, 3, 887–894.

Katongo C., Koller F., Ntaflos T., Koeberl Ch. & Tembo F., 2011: Occurrence and origin of scapolite in the Neoproterozoic Lufilian–Zambezi Belt, Zambia: Evidence/role of brine-rich fluid infiltration during regional metamorphism. *In:* J. Ray et al. (Eds.): Topics in Igneous Petrology, Springer Science-Business Media B.V., pp. 449–473, DOI:10.1007/978-90-481-9600-5-18.

Kerrick D.M., Crawford K.E. & Randazzo A.F., 1973: Metamorphism of calcareous rocks in three roof pendants in the Sierra Nevadas, California. *Journal of Petrology*, 14, 303–325.

Korinevsky V.G., 2015: Spessartine-andradite in scapolite pegmatite, Ilmeny Mountains, Russia. *Canadian Mineralogist*, 53, 623–632.

Korinevsky V.G. & Korinevsky E.V., 2016: Unusual shape of pyrrhotite inclusions in scapolite of igneous rocks from the Southern Urals. *Geology of Ore Deposits*, 58, 691–696.

Kuhn B.K., Reusser E. & Powell R., 2005: Metamorphic evolution of calc-schists in the Central Alps, Switzerland. *Schweizerische Mineralogische und Petrographische Mitteilungen*, 85, 175–190.

Kullerud K. & Erambert M., 1999: Cl-scapolite, Cl-amphibole, and plagioclase equilibria in ductile shear zones at Nusfjord, Lofoten, Norway: Implications for fluid compositional evolution during fluid-mineral interaction in the deep crust. *Geochimica et Cosmochimica Acta*, 63, 3829–3844.

Kusachi I., Osonai Y., Toyoshima T., Owada M., Tsunogae T., Hokada T. & Crowe W.A., 1999: Mineralogy of scapolite from Skallen in the Lützow-Holm Bay region, East Antarctica. *Polar Geoscience*, 12, 143–156.

Lafuente B., Downs R.T., Yang H. & Stone N., 2015: The power of databases: the RRUFF project. *In:* T. Armbruster, R.M. Danisi (Eds.): Highlights in Mineralogical Crystallography, Berlin, Germany, W. De Gruyter, pp. 1–30.

Larsen R.B., 1991: Tungsten skarn mineralizationn in a regional metamorphic terrain in southern Norway: a possible metamorphic ore deposit. *Mineralium Deposita*, 26, 281–289.

Lieftink D.J., Nijiland T.G. & Maijer C., 1993: Cl-rich scapolite from Ødegårdens Verk, Bamble, Norway. *Norsk geologisk tidsskrift*, 73, 55–57.

Macey P.H., Miller J.A., Rowe C.D., Grantham G.H., Siegfried P., Armstrong R.A., Kemp J. & Bacalau J., 2013: Geology of the Monapo Klippe, NE Mozambique and its significance for assembly of central Gondwana. *Precambrian Research*, 233, 259– 281.

Macey P.H., Thomas R.J., Grantham G.H., Ingram B.A., Jacobs J., Armstrong R.A., Roberts M.P., Bingen B., Hollick L., de Kock G.S., Viola G., Bauer W., Gonzales E., Bjerkgard T., Henderson I.H.C., Sandstad J.S., Cronwright M.S., Harley S., Solli A., Nordgulen Ø, Motuza G., Daudi E. & Manhica V., 2010: Mesoproterozoic geology of the Nampula Block, northern Mozambique: tracing fragments of Mesoproterozoic crust in the heart of Gondwana. *Precambrian Research*, 182, 124–148.

Madyukov I.A., Chupin V.P. & Kuzmin D.V., 2011: Genesis of scapolite from granulites (lower-crustal xenoliths from the Pamir diatremes): results of study of melt inclusions. *Russian Geology and Geophysics*, 52, 1319–1333.

Mathavan V. & Fernando G.W.A.R., 2001: Reactions and textures in grossular–wollastonite–scapolite calc–silicate granulites from Maligawila, Sri Lanka: evidence for high-temperature isobaric cooling in the meta-sediments of the Highland Complex. *Lithos*, 59, 217–232.

Millhollen G.L., 1974: Synthesis of scapolite under magmatic conditions. *American Mineralogist*, 59, 618–620.

Mittwede S.K., 1994: Primary scapolite in a granitic pegmatite, western Cherokee County, South Carolina. *Canadian Mineralogist*, 32, 617–622.

Moazzen M., Oberhänsli R., Hajialioghli R., Möller A., Bousquet R., Droop G. & Jahangiri A., 2009: Peak and post-peak P–T conditions and fluid composition for scapolite-clinopyroxene-garnet calc-silicate rocks from the Takab area, NW Iran. *European Journal of Mineralogy*, 21, 149–162.

Moecher D.P., Essene E.J. & Valley J.W., 1992: Stable isotopic and petrological constraints on scapolitization of the Whitestone meta-anorthosite, Grenville province, Ontario. *Journal of Metamorphic Geology*, 10, 745–762.

Mora C.I. & Valley J.W., 1991: Prograde and retrograde fluid-rock interactions in calcsilicates northwest of the Idaho Batolith - stable isotopic evidence. *Contributions to Mineralogy and Petrology*, 108, 162–174.

Mouchos E., Papadopoulou L., Williamson B.J. & Christofides G., 2016: Marialitic scapolite occurrences from the Kimmeria-Lefkopetra metamorphic contact, Xanthi (N. Greece). *Bulletin of the Geological Society of Greece*, 50, 1943–1951.

Mposkos E., 1978: Scapolite of Seriphos and the garnet composition of several garnetites of the island. *Bulletin of the Geological Society of Greece*, 13, 34–45 [In Greek].

Nabelek P.I., 2002: Calc-silicate reactions and bedding-controlled isotopic exchange in the Notch Peak aureole, Utah: implications for differential fluid fluxes with metamorphic grade. *Journal of Metamorphic Geology*, 20, 429–440.

Orville P.M., 1975: Stability of scapolite in the system Ab-An-NaCl-$CaCO_3$ at 4 kbar and 750°C. *Geochimica et Cosmochimica Acta*, 39, 1091–1105.

Oterdoom W.H., 1980: Scapolite in metamorphic calc-silicate rocks: Crystallographic and phase relations. PhD. Thesis, ETH Zürich, 134 p.

Oterdoom W.H. & Wenk H., 1983: Ordering and composition of scapolite: Field observations and structural interpretations. *Contribution to Mineralogy and Petrology*, 83, 330–341.

Owen J.V. & Greenough H.D., 1999: Scapolite pegmatite from the Minas fault, Nova Scotia: tangible manifestation of Carboniferous, evaporite-derived hydrothermal fluids in the western Cobequid highlands? *Mineralogical Magazine*, 63, 387–397.

Pan-Y., Fleet M.E. & Pay G.E., 1994: Scapolite in two Canadian gold deposits: Nickel Plate, British Columbia and Hemlo, Ontario. *Canadian Mineralogist*, 32, 825–837.

Pandit M.K., Carter L.M., Ashwal L.D., Tucker R.D., Torsvik T.H., Jamveit B. & Bhushan S.K., 2003: Age, petrogenesis and significance of 1 Ga granitoids and related rocks from the Sendra area, Aravalli craton, NW India. *Journal of Asian Earth Sciences*, 22, 363–381.

Pinna P., Jourde G., Calvez J.Y., Mroz J.P. & Marques J.M., 1993: The Mozambique Belt in northern Mozambique: Neoproterozoic (1100–850 Ma) crustal growth and tectogenesis, and superimposed Pan-African (800–550 Ma) tectonism. *Precambrian Research*, 62, 1–59.

Porter J.K. & Austrheim H., 2017: Sulphide formation from granulite-facies S-rich scapolite breakdown. *Terra Nova*, 29, 29–35.

Raith J.G. & Högelsberger H., 1994: Fluidentwicklung und Scapolithbildung in metamorphen Gesteinen der Saualpe. *Mitteilungen der Österreichischen Mineralogischen Gesellschaft*, 139, 165–168.

Ramsay C.R. & Davidson L.R., 1970: The origin of scapolite in the regionally metamorphosed rocks of Mary Kathleen, Queensland, Australia. *Contributions to Mineralogy and Petrology*, 25, 41–51.

Reznitsky L.Z., 1978: Mineral associations of magnesian skarns of the Slyudyanka phlogopite deposits. *In*: Shmakin B.M. (Ed): Mineralogy of Cisbaikalia (Guidebook for Baikal Excursions of the XIth General IMA Meeting), Irkutsk, 37–51 (Russian and English text).

Rosen O.M., Sidorenko S.A. & Kuznetsova N.N., 1977: Scapolite and apatite as indicators of composition of volatiles in metamorphism of the granulite complex of the Kola Peninsula. *Doklady of the Academy of Sciences of the U.S.S.R. Earth sciences section*, 237, 211–213.

Saintilan N.J., Selby D., Creaser R.A. & Dewaele S., 2018: Sulphide Re-Os geochronology links orogenesis, salt and Cu-Co ores in the Central African Copperbelt. *Scientific Reports*, 8, 14946, DOI:10.1038/s41598--018-33399-7.

Satish-Kumar M. & Harley L.S., 1998: Reaction textures in scapolite–wollastonite– grossular calc-silicate rock from the Kerala Khondalite Belt, Southern India: evidence for high-temperature metamorphism and initial cooling. *Lithos*, 44, 83–99.

Satish-Kumar M., Santosh M. & Yoshida M., 1995: Reaction textures in calc-silicates as guides to the pressure-temperature-fluid history of granulite facies terrains in East Gondwana. *Journal of Geosciences*, Osaka City University, 38, 89–114.

Schandl E.S., Gorton M.W. & Bray C.J., 2011: High-temperature brine in chalcopyriterich quartz vein 40 km southwest of Sudbury, Ontario. *Canadian Journal of Earth Sciences*, 48, 1369–1385.

Schenk V., 1984: Petrology of felsic granulites, metapelites, metabasics, ultramafics and metacarbonates from southern Calabria (Italy): prograde metamorphism, uplift and cooling of a former lower crust. *Journal of Petrology*, 25, 255–298.

Schmidt-Mumm A., Behr H.-J. & Horn E.-E., 1987: Fluid systems in metaplaya sequences in the Damara Orogen (Namibia): Evidence for sulfur-rich brines – General evolution and first results. *Chemical Geology*, 61, 135–145.

Schwarcz H.P. & Speelman E.L., 1965: Determination of sulfur and carbon coordination in scapolite by infra-red absorption spectrometry. *American Mineralogist*, 50, 656–666.

Searle M.P. & Cox J., 2002: Subduction zone metamorphism during formation and emplacement of the Semail ophiolite in the Oman Mountains. *Geological Magazine*, 139, 241–255.

Shaw D.M., 1960: The geochemistry of scapolite, Part I: Previous work and general mineralogy. Part II: Trace elements, petrology and general chemistry. *Journal of Petrology*, 1, 218–260, 261–285.

Shay K., 1975: Mineralogical zoning in a scapolite-bearing skarn body on San Gorgonio Mountain, California. *American Mineralogist*, 60, 785–797.

Siegfried P.R., 1999: The Monapo structure and intrusive complex – an example of large scale alkaline metasomatism in northern Mozambique. *In:* Stanley C.J. et al. (Eds.), *Mineral Deposits: Processes to Processing*. Balkema, Rotterdam, pp. 683–686.

Sivaprakash C., 1981: Petrology of calc-silicate rocks from Koduru, Andhra Pradesh, India. *Contributions to Mineralogy and Petrology*, 77, 121–128.

Smith G.C., Holness M.B. & Bunbury J.M., 2008: Interstitial magmatic scapolite in glass-bearing crystalline nodules from the Kula Volcanic Province, Western Turkey. *Mineralogical Magazine*, 72, 1243–1259.

Superchi M., Pezzotta F., Gambini E. & Castaman E., 2010: Yellow scapolite from Ihosy, Madagascar. *Gems & Gemology,* 46, 274–279.

Suzuki Y. & Nakai I., 1993: Marialite from Okaneda, Ibaragi Prefecture, Japan. *Geoscience Magazine*, 42, 135–142 [in Japanese].

Svenningsen O.M., 1994: The Baltica-Iapetus passive margin dyke complex in the Sarektjåkkå-Nappe, northern Swedish Caledonides. *Geological Journal*, 29, 4, 323–354.

Swart R., 1986: A note on an occurrence of scapolite in the northern zone of the Damara Orogen. *Communications Geological Survey of South West Africa/Namibia*, 2, 55–56.

Teertstra D.K., Schindler M., Sherriff B.L. & Hawthorne F.C., 1999: Silvialite, a new sulphate-dominant member of the scapolite group with an Al-Si composition near the *I*4/*m*-*P*42/*n* phase transition. *Mineralogical Magazine*, 63, 321–329.

Teertstra D.K. & Sherriff B.L., 1997: Substitutional mechanisms, compositional trends and end-member formulae of scapolite. *Chemical Geology*, 136, 233–260.

Torró L., Martin R.F., Schumann D., Cox J., Galí Medina S. & Melgarejo Draper J.C., 2018: The incipient flash melting of scapolite and plagioclase megacrysts in alkali basalts of the Olot suite, Catalunya, Spain, and at Chuquet Genestoux, Puy-de-Dôme, France. *European Journal of Mineralogy*, 30, 45–59.

Trommsdorff V., 1966: Progressive Metamorphose kieseliger Karbonatgesteine in den Zentralalpen zwischen Bernina und Simplon. *Schweizerische Mineralogische und Petrographische Mitteilungen*, 46, 431–460.

Ueda K., Jacobs J., Thomas R.J., Kosler J., Jourdan F. & Matola R., 2012: Delamination-induced late-tectonic deformation and high-grade metamorphism of the Proterozoic Nampula Complex, northern Mozambique. *Precambrian Research*, 196– 197, 275–294.

Vanko A.D. & Bishop F.C., 1982: Occurrence and origin of marialitic scapolite in the Humboldt lopolith, N.W. Nevada. *Contributions to Mineralogy and Petrology*, 81, 277–289.

Viola G., Henderson I.H.C., Bingen B., Thomas R.J., Smethurst M.A. & de Azavedo S., 2008: Growth and collapse of a deeply eroded orogen: insights from structural and geochronological constraints on the Pan-African evolution of NE Mozambique. *Tectonics*, 27, TC50009.

Warren R.G., Hensen B.J. & Ryburn R.J., 1987: Wollastonite and scapolite in Precambrian calc-silicate granulites from Australia and Antarctica. *Journal of Metamorphic Geology*, 5, 213–223.

Yoshino T. & Satish-Kumar M., 2001: Origin of scapolite in deep-seated metagabbros of the Kohistan Arc, NW Himalayas. *Contributions to Mineralogy and Petrology*, 140, 511–531.